THz field engineering in two-color femtosecond filaments using chirped and delayed laser pulses

A Nguyen, P González de Alaiza Martínez, I Thiele, Stefan Skupin, L Bergé

New Journal of Physics
The open access journal at the forefront of physics

Deutsche Physikalische Gesellschaft DPG IOP Institute of Physics

PAPER • OPEN ACCESS

THz field engineering in two-color femtosecond filaments using chirped and delayed laser pulses

To cite this article: A Nguyen *et al* 2018 *New J. Phys.* **20** 033026

New Journal of Physics
The open access journal at the forefront of physics

Deutsche Physikalische Gesellschaft DPG
IOP Institute of Physics

Published in partnership with: Deutsche Physikalische Gesellschaft and the Institute of Physics

OPEN ACCESS

RECEIVED
27 July 2017

REVISED
17 November 2017

ACCEPTED FOR PUBLICATION
29 December 2017

PUBLISHED
29 March 2018

PAPER

THz field engineering in two-color femtosecond filaments using chirped and delayed laser pulses

A Nguyen[1], P González de Alaiza Martínez[2], I Thiele[2], S Skupin[3] and L Bergé[1]

[1] CEA, DAM, DIF, F-91297 Arpajon, France
[2] Univ. Bordeaux—CNRS—CEA, Centre Lasers Intenses et Applications, UMR 5107, F-33405 Talence, France
[3] Institut Lumière Matière, UMR 5306 Université Lyon 1—CNRS, Université de Lyon, F-69622 Villeurbanne, France

E-mail: alisee.nguyen@cea.fr

Keywords: terahertz generation, chirp, plasma, filamentation, wave propagation

Abstract

We numerically study the influence of chirping and delaying several ionizing two-color light pulses in order to engineer terahertz (THz) wave generation in air. By means of comprehensive 3D simulations, it is shown that two chirped pulses can increase the THz yield when they are separated by a suitable time delay for the same laser energy in focused propagation geometry. To interpret these results, the local current theory is revisited and we propose an easy, accessible all-optical criterion that predicts the laser-to-THz conversion efficiencies given any input laser spectrum. In the filamentation regime, numerical simulations display evidence that a chirped pulse is able to produce more THz radiation due to propagation effects, which maintain the two colors of the laser field more efficiently coupled over long distances. A large delay between two pulses promotes multi-peaked THz spectra as well as conversion efficiencies above 10^{-4}.

1. Introduction

Terahertz (THz) time-domain spectroscopy is a promising way to analyze various complex materials, the molecular transitions of which possess unique fingerprints in this spectral range [1–3]. Amongst others, quite efficient methods to produce THz waves exploit laser-matter interaction processes and they rely on difference frequency generation in $\chi^{(2)}$ materials [4] or on more complex nonlinear processes in gas plasmas [5]. In the latter situation, a two-color ultrashort laser field composed of a fundamental harmonic (FH) frequency and its second harmonic (SH) ionizes the gas, which creates a plasma acting as frequency converter towards the THz range. However, to properly identify a material, the THz spectrum has to be tunable around selected frequencies and/or be broadband with high enough spectral intensity. Such versatility can be obtained from two-color gas plasmas, e.g., by increasing the fundamental laser wavelength [6, 7] or by employing incommensurate frequencies [8, 9].

Recently, the THz performances reached by optical rectification in organic crystals has been tremendously improved by chirping and combining delayed pulsed beams [10, 11]. The key idea is to employ temporally-modulated laser pulses over which the beam energy is appropriately distributed. This allows for a large tunability in the selection of THz oscillation cycles, central frequency and bandwidth over several octaves, whilst achieving strong laser-to-THz conversion efficiencies, high-field strengths >0.1 GV m^{-1}, and avoiding laser-induced material damage. Compared to crystal-based emitters, plasmas created in air by two-color femtosecond pulses are known to produce ultrabroadband THz pulses from photocurrents and they can deliver similar high-field strengths without being subject to any damage threshold. Another advantage of this technique is the ability to create THz emission at controlled remote distances by operating in the filamentation regime [12–14]. To render air-plasma emitters even more tunable and efficient, it is thus interesting to examine the actions of similar pulse-shaping techniques on photocurrents resulting from air ionization by two-color pulses. Chirping a single-pump pulse in two-color filaments has experimentally been shown to enhance THz generation [15]. Moreover, an increase in the THz generation was earlier numerically reported using particle-in-cell simulations of single-color

chirped pulses at high intensities [16]. Therefore, combining several consecutive two-color chirped pulses in a suitable manner should be a promising route towards even higher THz fields.

As known from the local current (LC) theory, photocurrents create broadband THz spectra that have been estimated so far from the product of the stepwise free electron density in tunnel regime and the accelerated electric field at the ionization instants [17]. In the present article, LC estimations predict that the THz yield of two-color chirped pulses can be dramatically enhanced when they are split into subpulses separated by an appropriate time delay. These predictions are confirmed by direct, comprehensive 3D simulations of focused beams that produce comparable orders of magnitude to the LC results in focused geometry. To understand this effect, we utilize a new criterion derived from the LC theory and based on the convolution product of the laser field and of the generated electron density in frequency domain. Given the spectrum of different input laser fields, the potential laser-to-THz conversion efficiency of the latter can be rapidly evaluated from the spectrum of the associated electron density at the main colors of the laser field. In the case of long-range propagation in collimated geometry, it is found that laser filamentation obscures the direct dependency of the THz spectra on the input pulse configuration. Nevertheless, two-color chirped filaments are shown to enhance locally the THz yield due to a better coupling between the FH and SH components over long propagation distances.

2. Chirping and delaying two-color pulses over short propagation ranges

To understand the action of chirped phases and delaying several pulses in time, we first perform LC estimates applied to a sequence of two-color chirped pulses. According to the LC model [5, 17], the THz field $\vec{E}_{\mathrm{THz}}$ is extracted from filtering in the THz window the secondary field $\vec{E}_J = g\partial_t\vec{J}$ emitted from the current density $\vec{J}$ induced by free electrons, g being a geometrical factor originating from Jefimenko's theory [18]. At moderate intensities $<10^{15}$ W cm^{-2}, the temporal shape of $\vec{J}$ is given by a plasma fluid model [5]:

$$\partial_t\vec{J} + \nu_c\vec{J} = \frac{e^2}{m_e}N_e\vec{E}, \tag{1}$$

where e and m_e are the electron charge and mass, respectively, and $\nu_c \approx 3$ ps^{-1} is the electron-neutral collision rate comparable to that assumed in filament setups [19, 20]. N_e is the density of free electrons governed by $\partial_t N_e = W(\vec{E})(N_a - N_e)$, where N_a is the initial gas density and $W(\vec{E})$ the field-dependent ionization rate. This rate is taken as the standard quasi-static tunnel rate of [2] applied to the single ionization of dioxygen molecules in air ($N_a = 5.4 \times 10^{18}$ cm^{-3}). More complex ionization models, including several species and multi-photon contributions, could be employed as well and would lead to similar qualitative behaviors for the pulse parameters examined here. Also, including additional THz sources such as, e.g., the Kerr response of air would be straightforward by just adding the second time-derivative of the third-order nonlinear polarization to the local THz source. However, this contribution is minor as soon as plasma generation sets in and THz generation from photocurrents takes over as reported in [20]. In our simplified model, the right-hand side of equation (1) is evaluated on the laser field $\vec{E}_L$ and the spatial distribution of $\vec{J}$ is shaped by a delta function. Applying these hypotheses to Jefimenko equations, the far-field power spectrum is then found to be proportional to the source term $N_e^L\vec{E}_L$, where $N_e^L \equiv N_e(\vec{E}_L)$. Equation (1) supplies the LC source for the far-field power spectrum

$$\hat{\vec{E}}_J(\omega) = \frac{ge^2}{m_e(1 + \mathrm{i}\nu_c/\omega)}\left(\hat{N}_e^L * \hat{\vec{E}}_L\right)(\omega), \tag{2}$$

where $*$ denotes the convolution product and hat symbol is the Fourier transform in time.

The input light field is taken as

$$\vec{E}_L(t) = E_0\sum_{k=0}^{K-1}\sum_{n=1}^{N}F\left(\frac{t_k}{\tau_n}\right)\vec{a}_n\cos\left(n\omega_0 t_k + \phi_n + 2C_n\ln 2\frac{t_k^2}{\tau_n^2}\right), \tag{3}$$

where $E_0 = \sqrt{2I_0/c\epsilon_0}$ depends on the pump intensity I_0, ω_0 is the FH frequency ($n = 1$), $t_k \equiv t - k\Delta t$ and $\vec{a}_n = a_n\vec{e}_n$ with a_n and $\vec{e}_n$ being the amplitude coefficient and unit vector fixing the polarization state of the nth harmonic, respectively. Equation (3) models a general pulse field composed of K identical subpulses delayed from each other by Δt. We choose Gaussian envelopes, $F(u) = \exp(-2\ln 2\ u^2)$ and the fundamental wavelength $\lambda_0 = 2\pi c/\omega_0$ is $\lambda_0 = 800$ nm. Each pulse contains N colors (harmonics) with mutual phase angles ϕ_n. The overall pulse fluence $\mathcal{E}_{\mathrm{in}} \equiv \frac{1}{2}c\epsilon_0\int_{-\infty}^{+\infty}|E_L(t)|^2\mathrm{d}t$ is maintained constant, so that, depending on the number and mutual spacing of the K pulses, the maximum intensity may vary from one pulse configuration to another one.

Concerning the duration of the harmonics and their associated chirp factors, different options can be considered. For instance, each pulse can contain the same full-width-at-half-maximum (FWHM) duration $\tau_n = \tau$ subject to the same chirping through the parameter $C_n = C$. This choice guarantees that the input spectra of both FH and SH have the same bandwidth with or without chirp. However, the relative phase between

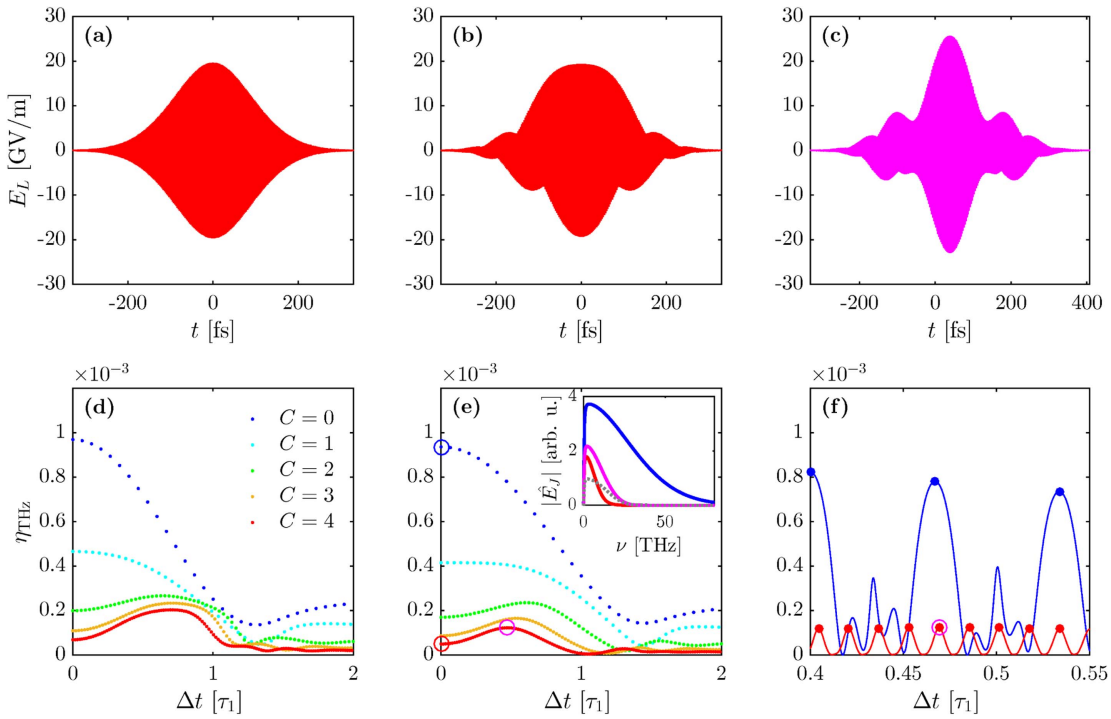

Figure 1. (a)–(c) Laser field profiles of equation (3) with $K = N = 2$, $a_1 = \sqrt{0.9}$, $a_2 = \sqrt{0.1}$, $\phi_1 = 0$, $\phi_2 = \pi/2$, $C_1 = C_2 \equiv C = 4$, and $\tau_1 = \sqrt{1 + C^2}\tau_0$ with $\tau_0 = 40$ fs for (a) $\tau_2 = \tau_1/\sqrt{2}$, $\Delta t = 0$, (b) $\tau_2 = \tau_1$, $\Delta t = 0$ or (c) $\tau_2 = \tau_1$, $\Delta t = 0.47\tau_1$. The pulse fluence is constant (3.6 J cm^{-2}). (d)–(f) Conversion efficiency η_{THz} (equation (4)) versus the time delay between two pulses discretized in units of FH optical cycles $2\pi/\omega_0$ for different chirp values and (d) $\tau_2 = \tau_1/\sqrt{2}$ or (e) $\tau_2 = \tau_1$. The three colored circles represent the configurations further simulated when using the 3D UPPE model equation (6). The three associated spectra using equation (2) are plotted in the inset. The gray dotted line represents the spectrum for $C_1 = C_2 = 4$ and $\Delta t = 0.4\tau_1$. (f) Zoom of (e) over delay values covering the Δt range continuously.

the pulse components varies along the pulse, which can be detrimental to optimum THz pulse generation. Reciprocally, preventing the relative phase between the harmonics from varying in time may not keep the spectral contents of all colors equal when chirping their respective phase, which can render an efficient overlap of the subpulses more difficult to tune. For this purpose, figures 1(a)–(c) illustrate two-color laser fields involving two distinct pulses ($K = 2$) with different parameter values for C_n, τ_n and delay Δt. Figure 1(a) shows two superimposed ($\Delta t = 0$) dual-color pulses with $\tau_2 = \tau_1/\sqrt{2}$, $C_2 = C_1 = 4$, $\tau_1 \simeq 165$ fs and $\tau_2 \simeq 117$ fs, which is representative of the canonical situation where the SH is produced through a frequency doubling (e.g., BBO) crystal [17]. Here the $\pi/2$ phase angle between FH and SH is constant along the pulse, but the spectral broadening is not the same for the two colors. For comparison, another configuration using $C_2 = C_1 = 4$ and $\tau_2 = \tau_1 \simeq 165$ fs, again with $\Delta t = 0$, is plotted in figure 1(b). This configuration cannot preserve the phase angle along the entire pulse (except near the pulse center), but it keeps the same spectral width for the FH and SH pulses. Figure 1(c) shows the same combination of pulses when introducing a non-zero time delay $\Delta t = 0.47\tau_1$, which corresponds to an optimum number of optical cycles that increases the peak field strength and provides an overall pulse with a shorter FWHM duration.

To foresee the best laser configurations, an estimate of the laser-to-THz conversion efficiency is defined as

$$\eta_{\mathrm{THz}} \equiv \int_0^{2\pi\nu_{\mathrm{THz}}} \left|\widehat{E}_J\right|^2 \mathrm{d}\omega \Big/ \int_0^{+\infty} \left|\widehat{E}_L\right|^2 \mathrm{d}\omega, \tag{4}$$

where the numerator is computed from equation (2) with $\nu_{\mathrm{THz}} = 80$ THz. Indeed it should be recalled in this respect that, due to the unknown geometrical factor g, the LC source field $\widehat{E}_J$ in equation (2) cannot provide any quantitative evaluation of the produced field strength. However, here we are only interested in the relative variations that can be expected in laser-to-THz conversion efficiencies from one pulse configuration to another one. In addition, we wish to estimate these variations keeping into account that, for a class of pulse configurations with same input energy, plasma defocusing in three-dimensional (3D) propagation geometries clamps the achieved peak intensity, which, by feedback, constrains the maximum electron density to comparable levels or similar ionization degrees [7]. Therefore, we shall choose the factor g as providing a convenient normalization with respect to the maximum density of the generated free electrons, i.e.

$$g = \frac{m_e}{e^2 \max_t N_e^L}. \tag{5}$$

For the sake of readability, we also adjust equation (4) to the value of the conversion efficiency numerically computed from a 3D simulation of a basic unchirped pulse with no delay.

Equation (4) is plotted in figures 1(d), (e) in terms of the chirp parameter taken equal for every pulse component, $C_1 = C_2$, and delay value Δt. In this figure η_{THz} is represented for a delay Δt discretized in units of the FH optical cycle $2\pi/\omega_0$ for the same input fluence of 3.6 J cm^{-2}. The second color duration is chosen as $\tau_2 = \tau_1/\sqrt{2}$ in figure 1(d) and $\tau_2 = \tau_1$ in figure 1(e). We can observe that the laser-to-THz conversion efficiency remains quite comparable between these two classes of pulses. Despite slightly better conversion values promoted by a constant phase angle across the pulse, the THz energy yields remain of the same order for the two pulse configurations. For the sake of simplicity, in particular for measuring time delays Δt in terms of identical optical cycles in FH and all the harmonics, we shall henceforth choose the configuration $C_2 = C_1 \equiv C$ and $\tau_2 = \tau_1 \equiv \tau$. In the following, all pulse components have the same FWHM duration $\tau = \sqrt{1 + C^2}\tau_0$ with transform-limited duration $\tau_0 = 40$ fs. In figure 1(e) we report an increase in the efficiency whenever $\Delta t = 0.47\ \tau$ when using a chirp factor $C = 4$, which corresponds to 29 optical cycles. Importantly, in order to achieve a high THz yield, Δt has to be an integer number of optical cycles. Indeed, figure 1(f) zooms on the small-scaled variations in the laser-to-THz conversion efficiency, when Δt is no longer an integer value of $2\pi/\omega_0$. This figure then reveals finer modulations in η_{THz} when Δt is continuously varying in time. These indicate that, to optimize the THz yield from photocurrents, an accurate control of the delay between the two pulses within the interval of one optical cycle is necessary. For comparison, the inset of figure 1(e) shows the net decrease in the THz spectrum with a delay of $\Delta t = 0.4\ \tau$ (see gray dotted curve), which corresponds to a non-integer number of optical cycles. Moreover, as can be seen in figure 1(e), the optimum delay does depend on the chirp value. Comparing this figure with figure 1(d) reveals that the optimum delay also varies with the SH pulse duration (to a lesser extent), as well as with the phase between the two colors (not shown).

In order to confirm our expectations, we employ the 3D unidirectional pulse propagation equation [21, 22]:

$$\partial_z \hat{E} = \mathrm{i}\sqrt{k^2(\omega) - k_x^2 - k_y^2}\ \hat{E} + \mathrm{i}\frac{\mu_0 \omega^2}{2k(\omega)}\hat{\mathcal{F}}_{\mathrm{NL}}, \tag{6}$$

where $k(\omega) = n(\omega)\omega/c$ is the wave number [$n(\omega)$ and c are the refraction index and speed of light in vacuum, respectively], z is the propagation variable and $\hat{E}(k_x, k_y, z, \omega)$ is the Fourier transform of the electric field $E(x, y, z, t)$. The first term on the right-hand side of equation (6) describes linear dispersion and diffraction of the pulse. The second term $\hat{\mathcal{F}}_{\mathrm{NL}} = \hat{P}_{\mathrm{NL}} + \mathrm{i}\hat{J}/\omega + \mathrm{i}\hat{J}_{\mathrm{loss}}/\omega$ contains the third-order nonlinear polarization P_{NL}, the electron current J and a loss term J_{loss} due to ionization [23]. Air dispersion is taken from [24], while the Kerr index for self-focusing is $n_2 = 3.8 \times 10^{-19}$ cm^2 W^{-1} with 80% of Raman-delayed response [25, 26]. Instead of using the elementary quasi-static tunnel rate, our numerical model employs the Perelomov, Popov and Terent'ev's ionization rate [27] applied to 80% of dinitrogen and 20% of dioxygen for the sake of completeness.

We first study the effects of pulse chirping and inter-pulse delay in a focused propagation, using a converging lens of focal length $f = 2.5$ cm.

Three simulations have been performed, using one transform-limited pulse ($C = 0$, $\tau = 40$ fs), and two chirped pulses ($C = 4$, $\tau \simeq 165$ fs) with $\Delta t = 0$ and $\Delta t = 0.47\tau$, as suggested by figures 1(e), (f). The initial field is given by equation (3) ($K = N = 2$) for Gaussian transverse profiles with input width $w_0 = 0.5$ mm (see, e.g., [28]) and 0.2 mJ energy with 10% of SH. Both FH and SH input pulses have the same absolute spectral content in the chirped or unchirped configurations. Figure 2(a) shows the numerical counterpart of equation (4), computed from the 3D-simulated THz field that is extracted from the overall electric field filtered in the THz window of interest ($\nu < 80$ THz) along the propagation path. The growth in the THz conversion efficiency achieved near focus is in good qualitative agreement with our LC-based conversion efficiency, including the gain factors. From a more quantitative point of view, the pulse propagation amplifies the maximum conversion efficiencies up to 10^{-3}. Introducing a delay into identically-chirped pulses can increase by a factor ~5 the resulting THz energy computed for $\nu < 80$ THz (figure 2(a)), which directly impacts the THz field strength (figure 2(b)). Figures 2(c)–(e) detail the propagation of the THz spectra averaged over the transverse direction and limited to the 20 THz range. These follow the trends shown in the inset of figure 1(e). The THz spectral width and intensity being linked to the number of cycles in the laser field ($\Delta\nu_{\mathrm{THz}} \propto 1/\tau$), the chirped pulses exhibit narrower bandwidth and weaker field strengths. However, delaying them by 0.47τ (see figure 2(e)) substantially amplifies the THz spectrum and the emitted field, as previously expected from figure 1(e). Note in figure 2(b) that the THz field with $C = 0$ resulting from a broader THz spectrum develops higher frequencies than those produced by the chirped pulses.

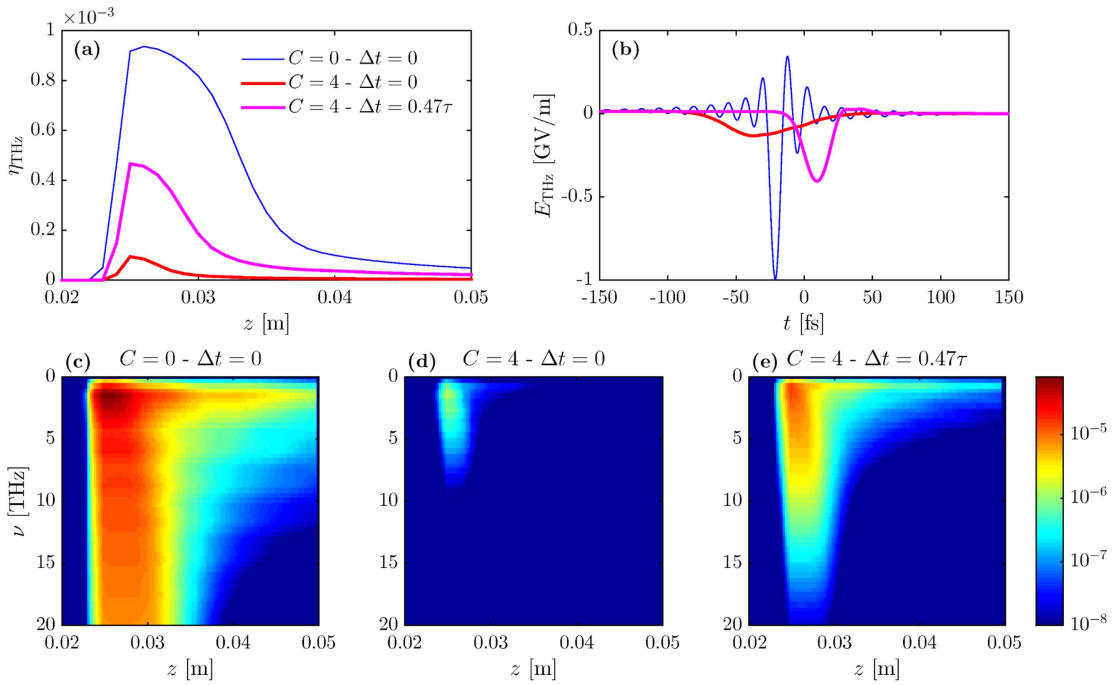

Figure 2. (a) Laser-to-THz conversion efficiency along propagation from UPPE simulations in focused regime ($f = 2.5$ cm) with $C = 0$, $\tau = 40$ fs (blue curve), $C = 4$, $\tau \simeq 165$ fs, $\Delta t = 0$ (red curve) and $C = 4$, $\tau \simeq 165$ fs, $\Delta t = 0.47\tau$ (magenta curve). (b) Corresponding on-axis THz fields near focus ($z = 2.4$ cm) filtered in the frequency range $\nu < 80$ THz using a step function. (c)–(e) Transversally-averaged spectral intensity (in arbitrary units) along propagation for (c) $C = 0$, (d) $C = 4$, $\Delta t = 0$ and (e) $C = 4$, $\Delta t = 0.47\tau$.

3. An 'optical' criterion to evaluate the laser-to-THz conversion efficiency

To explain the previous results, we develop a purely optical model based on the LC theory that discards propagation effects. By 'optical model', it is meant that only the spectral contents of the input laser field and associated electron density at the optical frequencies are utilized to evaluate and justify the changes in the laser-to-THz conversion efficiency. Instead of exploiting electron velocity fields at the ionization instants as in [7, 8, 29], we focus on the convolution product of $\widehat{N}_e^L$ and $\widehat{\vec{E}}_L$ around the main harmonics of the optical pulse.

To start with, let us ignore the influence of the Gaussian pulse envelopes. We first select an unchirped two-color laser field having a square-shaped envelope $E_L(t) = 0$ for $|t| > \tau/2$, where the FWHM duration τ is identical for all subpulses. We also omit the vectorial nature of the pump field for which, except in contrary case, we assume identical (linear) polarization of all pulse components. The spectrum of the input field then decomposes over the sum of distributions centered at $\omega = \pm n\omega_0$ and modulated by the interference pattern of the K subpulses, namely

$$\hat{E}_L(\omega) = E_0 \frac{\tau}{2} \mathrm{e}^{\mathrm{i}(K-1)\omega\frac{\Delta t}{2}} \frac{\sin(K\omega\Delta t/2)}{\sin(\omega\Delta t/2)} \sum_{\pm} \sum_{n=1}^{N} a_n \mathrm{e}^{\pm \mathrm{i}\phi_n} \mathrm{sinc}\left(\frac{\tau}{2}(\omega \pm n\omega_0)\right). \tag{7}$$

Plugging this ansatz into the convolution integral

$$\widehat{N}_e^L * \widehat{E}_L(\omega) = \int_{-\infty}^{+\infty} \widehat{N}_e^L(\omega - \omega')\widehat{E}_L(\omega')\mathrm{d}\omega' \tag{8}$$

immediately shows that this integral builds from the spectral components of the electron density at frequencies $\omega \pm n\omega_0$:

$$\left|\widehat{N}_e^L * \widehat{E}_L(\omega)\right| \approx \pi E_0 \left| \sum_{\pm} \sum_{n=1}^{N} a_n \mathrm{e}^{\pm \mathrm{i}\phi_n} \frac{\sin(nK\omega_0\Delta t/2)}{\sin(n\omega_0\Delta t/2)} \widehat{N}_e^L(\omega \pm n\omega_0) \right|. \tag{9}$$

In equation (9) we applied the approximation of many-cycles pulses $\omega_0\tau \gg 1$, i.e., $(a/\pi)\mathrm{sinc}(ax) \to \delta(x)$ with $a \to +\infty$, yielding a pulse spectrum being highly peaked at the optical frequencies, whereas the spectrum of N_e^L exhibits broader extents around the same frequencies. Looking at the low-frequency range, $\omega \ll \omega_0$, implies that the THz spectrum should be mainly determined by (i) the optical spectrum, which is known from the input pulse, and (ii) the spectrum of the free electron density evaluated at the optical harmonics within their corresponding bandwidths. Let us notice that equation (9) readily explains the loss of THz efficiency illustrated

by figure 1(f) when Δt differs from integer values of $2\pi/\omega_0$, which follows from destructive interferences described by the ratio of the two sine functions.

Repeating the previous reasoning when accounting for Gaussian pulse envelopes cannot, however, be done so directly. Nonetheless, we may still get some useful insights for small frequencies. First, since E_L and N_e^L are real functions, their Fourier transforms have even real and odd imaginary parts, and thus the knowledge of the spectra for $\omega \geqslant 0$ is sufficient. We can then make use of the Taylor expansion $f(\omega' - \omega) = \sum_j (-\omega)^j \partial^j_{\omega'} f(\omega')/j!$ in the convolution integral equation (8) to evaluate

$$\left|\widehat{E}_L * \widehat{N}_e^L\right|_{\omega\to 0} = 2\left|\int_0^{+\infty} [\hat{R}(\omega') + \hat{I}(\omega')]\,\mathrm{d}\omega'\right| + O(\omega^2), \tag{10}$$

where $\hat{R} \equiv \mathrm{Re}(\widehat{N}_e^L)\mathrm{Re}(\widehat{E}_L)$ and $\hat{I} \equiv \mathrm{Im}(\widehat{N}_e^L)\mathrm{Im}(\widehat{E}_L)$. It should be noted that, compared with a plane wave field limiting the validity range of our analysis to $\omega \ll \omega_0$, our equation (10) applying to optical pulses with smooth temporal profile is in principle valid only if the spectrum of $N_e^L E_L$ is peaked near $\omega = 0$. In equation (10) the ordering $O(\omega^2)$ follows from taking the square modulus of the real part of $\widehat{E}_L * \widehat{N}_e^L$ scaling as $\sim O(1)$ at leading order and of the ω-dependent imaginary part involving crossed (Re–Im) contributions. Applying a direct Taylor expansion for small ω when taking the square root then preserves the dependency in $O(\omega^2)$ of the modulus in equation (10).

Neglecting second-order contributions in ω^2, we sum up the integrands of equation (10) around the pulse frequencies within a small interval, e.g., $\epsilon = \pm\omega_0/10$, representative of the FH spectral broadening. This leads us to extract an efficiency factor in amplitude being dimensionless and normalized consistently with equation (5) as

$$\gamma_{\mathrm{THz}} \approx \frac{2\left|\sum_n \int_{n\omega_0-\epsilon}^{n\omega_0+\epsilon} [\hat{R}(\omega) + \hat{I}(\omega)]\,\mathrm{d}\omega\right|}{\max_t N_e^L \sqrt{\mathcal{E}_{\mathrm{in}}}}. \tag{11}$$

To visualize better the separated weights of the real and imaginary contributions, we treat this quantity only from the modulus of the convolution product, which amounts to evaluating somehow the square root of equation (4).

Equation (11) is the main result of our analytical approach. It signifies that the only knowledge of the real and imaginary parts of the input laser spectrum and of its associated plasma response at the optical frequencies can help sort out the most efficient pulse configurations for THz generation.

As a first example, figure 3(a) shows the efficiency factor γ_{THz} plotting separately the integrals of $\hat{R}$ and $\hat{I}$ for a classical two-color pulse with $\phi_1 = 0$. We retrieve the best SH phase angle $\phi_2 = \pi/2$ for THz production by photocurrents [30], which induces a substantial increase in $\hat{N}_e^L$ at FH frequency, hence in $\hat{R}$. Indeed, if we apply the approximation that ionization occurs at the maxima of E_L^2 and neglect the envelope effects, $N_e^L \approx \int_{-\infty}^{t} W(|E_L|)\,\mathrm{d}t \propto \int_{-\infty}^{t} E_L^2\,\mathrm{d}t$, we find that $\gamma_{\mathrm{THz}} \propto a_1^2 a_2 \sin(\phi_2 - 2\phi_1)/\omega_0$. For an arbitrary number N of colors, applying the same approximations to the general input field equation (3) with no chirp reveals the existence of direct-current components from a four-wave coupling scheme involving the product of the field amplitudes a_n, a_m, a_k whenever $k = n + m$, which yields

$$\gamma_{\mathrm{THz}} \propto \frac{1}{\omega_0}\sum_{n=1}^{N-1}\sum_{m=1}^{N-n} a_n a_m a_{n+m} \sin(\phi_n + \phi_m - \phi_{n+m})\left(\frac{1}{n+m} - \frac{2}{m}\right). \tag{12}$$

Another example illustrates in figure 3(b) the spectrum of the electron density computed on the first harmonics of a sawtooth wave shape, known to supply the highest THz yields to date at fixed ionization level [29]. For such waveforms, equation (3) consists of a single pulse ($k = 0$) involving an increasing number of harmonics with $a_n = 1/n$ and $\phi_n = (-1)^n\pi/2$. The Fourier transform of the laser field is then purely imaginary with alternating signs, so that the gain in THz performances is simply given by the most optimal distribution of the imaginary part of $\widehat{N}_e^L$ at the optical frequencies. The more the number of harmonics, the higher the electron density spectrum at FH frequency. Moreover, if the number of colors is augmented (here up to eight), the harmonics in $\widehat{N}_e^L$ get alternating signs and relative amplitudes, which coincide better and better with those of the pulse spectrum and thereby enhance even more the THz yield. This enhancement is consistent with that reported in [29]. This property can also be retrieved from implementing the amplitudes a_n and phase values ϕ_n of a sawtooth wave field into the gain factor equation (12).

A last example displayed in figure 3(c) concerns the vectorial nature of a two-color pump field exhibiting a $\pi/2$ relative phase. Here, we consider the polarization effects between two colors whose vectorial components, $\vec{a}_1 = a_1(1,\,0)$, $\vec{a}_2 = a_2(\cos\alpha,\,\sin\alpha)$, can be varied from parallel to orthogonal directions. When the polarization angle α is increased from 0 to $\pi/2$, the FH component in the electron density vanishes. The ionization events indeed occur at the maxima of $E_L^2(t)$, whose FH component is given by

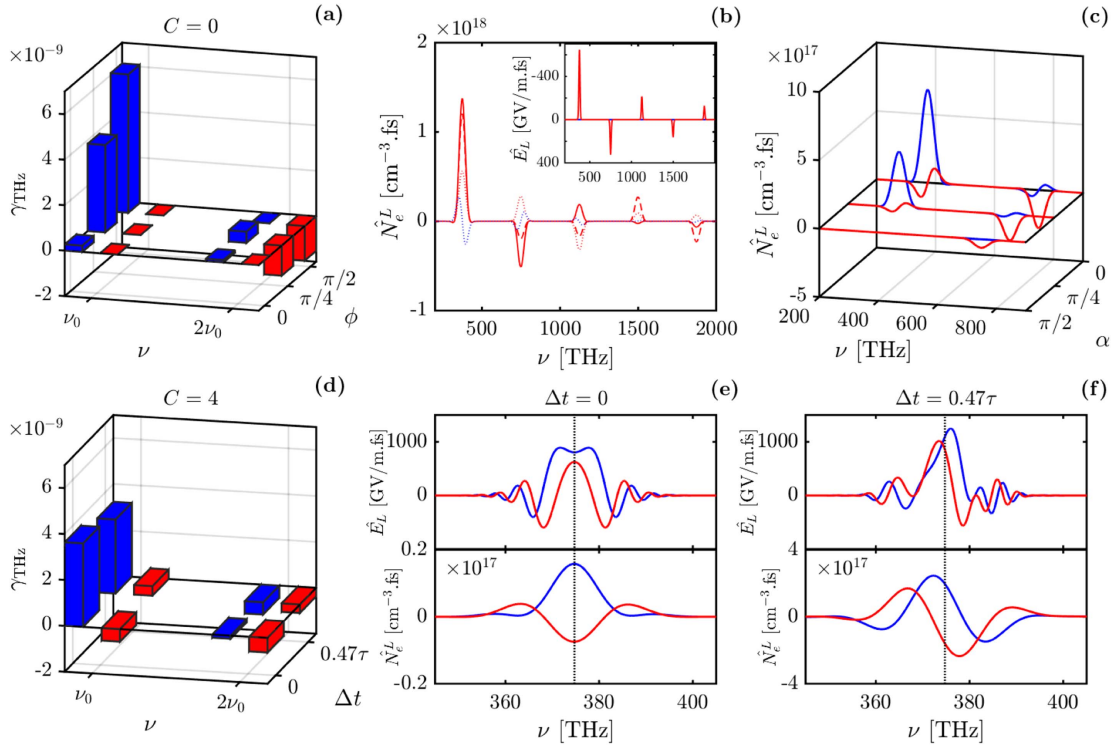

Figure 3. Integrals of real ($\hat{R}$) and imaginary ($\hat{I}$) contributions of equation (11) are plotted with blue and red boxes or curves, respectively. (a) THz efficiency factor (equation (11)) for relative phases of 0, $\pi/4$ and $\pi/2$ for two-color unchirped Gaussian pulses. (b) Electron density spectra (imaginary part) for a sawtooth profile approached by two (dotted), four (dashed) or eight colors (solid line). Inset shows $\hat{E}_L$. The blue dotted line plots the real part of the density spectrum for eight colors. (c) Electron density spectra for two colors with a polarization angle α between FH and SH varying from 0 to $\pi/2$. The relative phase is set equal to $\pi/2$ ($\phi_1 = 0,\ \phi_2 = \pi/2$) . (d) THz efficiency equation (11) for two chirped pulses ($C = 4$) being superimposed or delayed by 0.47τ. (e), (f) Laser field (top) and electron density (bottom) spectra around FH frequency for two chirped pulses ($C = 4$) being (e) superimposed or (f) delayed by 0.47τ.

$E^2_{L,\mathrm{FH}}(t) \propto E_0^2 a_1 a_2 \cos(\omega_0 t + \pi/2)\cos\alpha$. The efficiency factor then reads in vectorial form $\vec{\gamma}_{\mathrm{THz}} \propto a_1^2 a_2 \omega_0^{-1}(3\cos\alpha,\ -\sin\alpha)$. So, a dramatic fall of the THz yield occurs when FH and SH have crossed polarizations, which has recently been reported in [31, 32].

We next compute our efficiency factor (11) for the pulse configuration of figures 1(e) and 2(a), i.e., for two chirped pulses with $C = 4$, being either superimposed ($\Delta t = 0$) or delayed ($\Delta t \neq 0$). These two-color pulses have the same energy and $\pi/2$ relative phase. The time delay is again chosen as $\Delta t = 0.47\tau$, in order to match the optical cycles in the temporal domain where the two delayed pulses overlap. When one compares figures 3(a), (d), the amplitude efficiency factor γ_{THz} with $\Delta t = 0$ is found smaller for a chirped pulse ($C \neq 0$) due to its longer pump duration. However, we retrieve that its content becomes noticeably increased by introducing a time delay close to $\tau/2$, as evidenced by figure 3(d). Here, a positive contribution $\hat{I}$ increases γ_{THz} at the FH frequency. The detail of the convolution product, equation (10), is shown around the FH frequency in figures 3(e), (f). When two chirped pulses are delayed by $\Delta t = 0.47\tau$, the imaginary part of $\hat{N}_e^L$ has mostly the same sign as that of $\hat{E}_L$. $\hat{I}$ becomes positive and increases around the FH component, making the total yield greater than the one for $\Delta t = 0$. Therefore, higher THz components are produced, which justifies the gain reported in figure 1(e).

In summary, equation (11) provides useful information on the low-frequency part of the spectrum, assuming a concentration of THz components in the range $\omega/\omega_0 \ll 1$.

4. Chirped and delayed pulses in the filamentation regime

Let us now examine longer propagation ranges by simulating two-color laser filaments. The laser and medium parameters are identical to the former ones, except that the initial beam width is set to 1 mm. Propagation is collimated ($f = +\infty$) and the laser energy is increased to 4.5 mJ with 10% in SH. As evidenced in figure 4(a), pulse chirping, by increasing the pulse duration and thus the number of time slices subject to self-focusing and ionization, is able to enhance the self-channeling range, and thereby the zone of active plasma generation [33]. Although transform-limited pulses promote the highest plasma densities and the broadest spectra, chirped

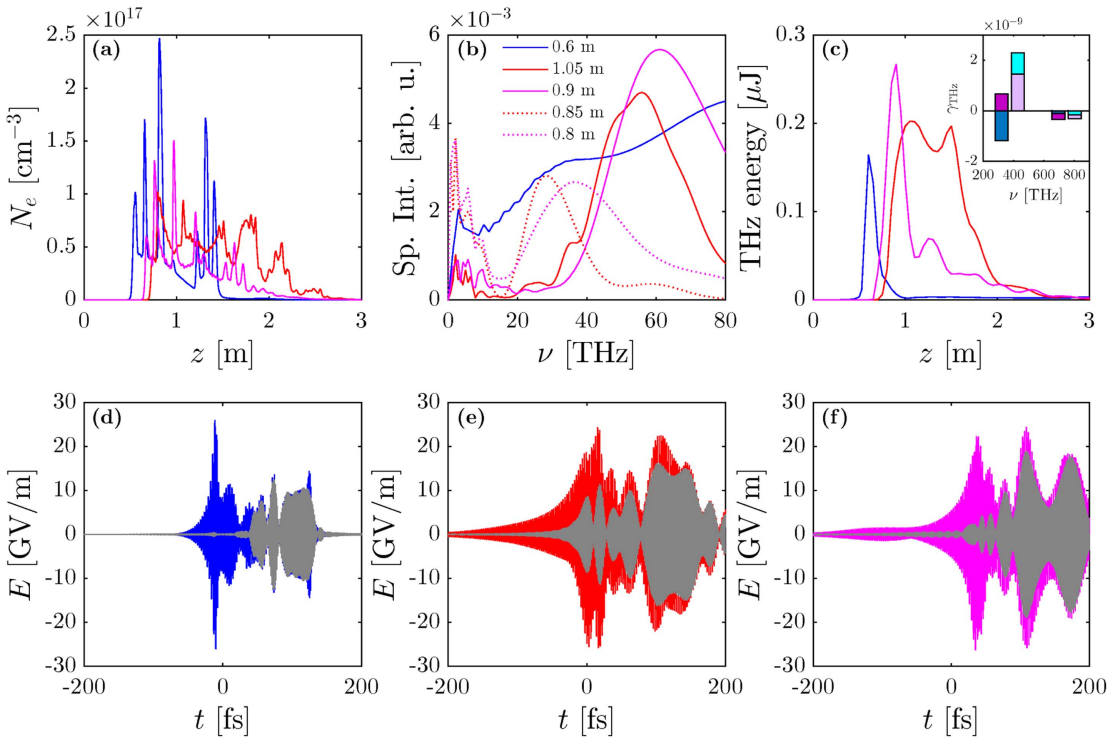

Figure 4. 3D UPPE simulations in filamentation regime with $C = 0$ (blue curves), $C = 4$, $\Delta t = 0$ (red curves) and $C = 4$, $\Delta t = 0.47\tau$ (magenta curves). (a) Peak electron density, (b) averaged spectral intensity at maximum THz emission, and (c) THz energy along propagation ($\nu < 80$ THz). The inset shows γ_{THz} for $C = 0$ (dark/light blue squares) and $C = 4$ (dark/light violet squares) with $\Delta t = 0$ computed from the numerical data files of the spectra of the electric field and electron density at distances of maximum THz generation (dark and light colored areas refer to the contributions $\widehat{R}$ and $\widehat{I}$, respectively). (d)–(f) Laser fields (FH +SH) at $z = 1$ m (blue, red or magenta areas) with corresponding SH component (gray areas) for (d) $C = 0$, (e) $C = 4$, $\Delta t = 0$ and (f) $C = 4$, $\Delta t = 0.47\tau$.

pulses help select a narrower THz window centered, e.g., around 60 THz in figure 4(b). Note that in this subplot the low-frequency THz peaks ($\nu \to 0$) are, however, partly suppressed because of the finiteness of the numerical box [7]. The smallest frequencies escape the box in the transverse direction over long propagation ranges. Chirped pulses retard the Kerr self-focusing since their input power varies as $P_C = P_{C=0}/\sqrt{1 + C^2}$. They accumulate more THz energy at long propagation distances (see figure 4(c)), where the maximum THz energy now exceeds that delivered by the unchirped pulse. This is again supported by the efficiency factor γ_{THz} (equation (11)) computed from our numerical data at maximum THz emission (see inset), which dramatically increases near the FH frequency for $C = 4$. The THz yield becomes even more enhanced when one introduces a time delay of 0.47τ between two chirped pulses (magenta curve). These properties are evidenced by figure 4(b), where the solid lines represent the THz spectra computed at maximum emission for a 80 THz window. Because THz radiations escape the transverse box along propagation, chirped pulse spectra computed at shorter distances that maximize the 20 THz range have also been plotted in dotted lines (this distance remains unchanged for $C = 0$). They again confirm the previous statements. The increase in the THz yield by chirped pulses is physically explained by the temporal drift of the second color inside the total field. Indeed, the temporal overlap between the two colors of the unchirped laser field is lost after propagation over ~1 m (figure 4(d)), as the group velocity mismatch ($\simeq 81$ fs m^{-1}) between the 800 and 400 nm pulses is rather large. In contrast, because phase chirping enlarges the pulse duration, an effective temporal overlap can be maintained over longer distances when adding a chirp, as can be seen in figure 4(e). A better coupling at the highest field extrema is even achieved when one initially delays the two chirped pulses (figure 4(f)).

In contrast to the THz performances of focused pulses that propagate over centimeter-ranges (see figure 2(a)), employing chirped and delayed pulses self-channeling over meter-range distances is able to increase the THz energy yield compared to transform-limited pulses (figure 4(c)). We attribute this property to a more efficient supercontinuum generation of the optical components due to self-phase modulation that enriches the THz spectrum over long distances. An illustrative example is given in figure 5, which shows the pulse spectra corresponding to figures 2(d), (f) and to 4(d), (f) for short- and long-range propagations, respectively, in the cases $C = 0$, $\Delta t = 0$ and $C = 4$, $\Delta t = 0.47\tau$. The THz spectrum, which is inhibited by pulse chirping over short distances in focused geometry, significantly benefits from a better coupling between broadened spectral components over an extended filamentation range.

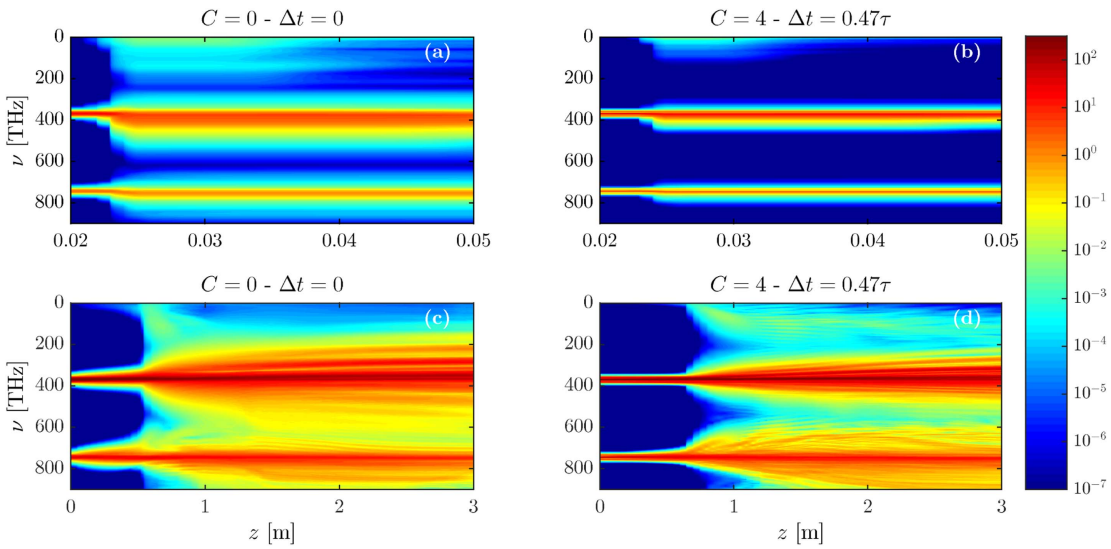

Figure 5. Optical spectra for the focused two-color pulses of figure 2 with (a) $C = 0$, $\Delta t = 0$ and (b) $C = 4$, $\Delta = 0.47\tau$. (c), (d) Same information for the pump pulses of figure 4 propagating in filamentation regime. The color bar specifies the spectral intensity levels (arbitrary units).

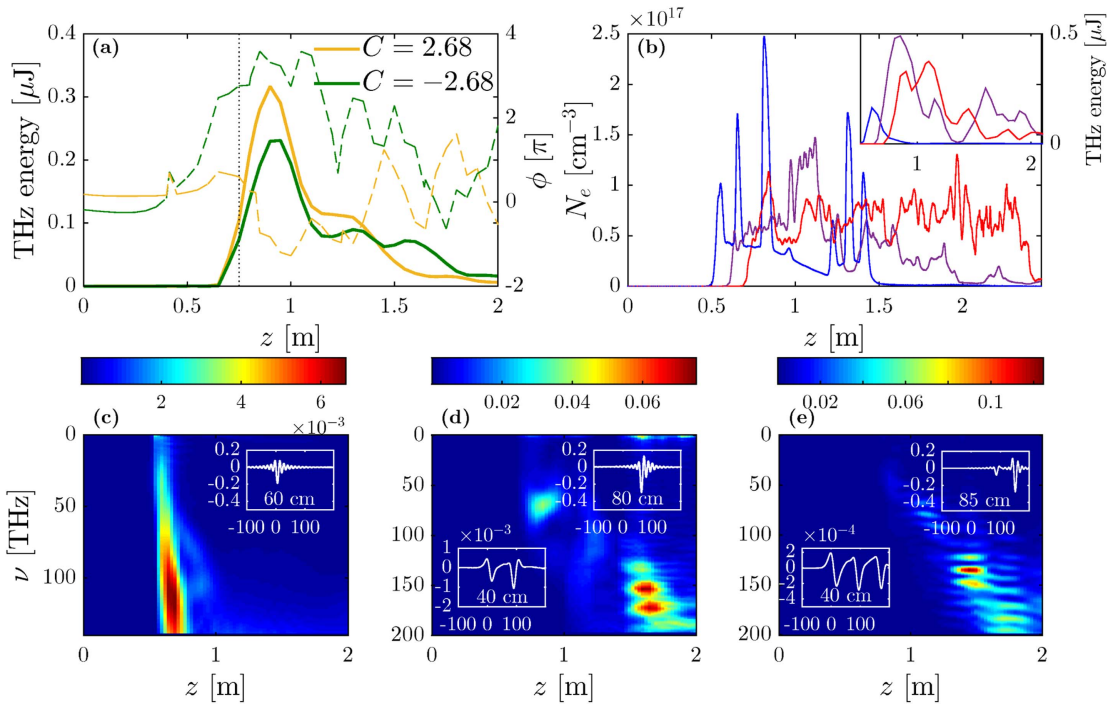

Figure 6. (a) THz yield (solid curves) and relative phase (dashed curves) along propagation of a single pulse with $C = 2.68$ (yellow curves) and $C = -2.68$ (green curves). The vertical dotted line points out the distance of maximum THz production. (b) Electron density for $C = 0$ with one (blue curve), two (violet curve) or three pulses (red curve) separated by 2τ. Inset shows the associated THz energy yield ($\nu < 80$ THz). (c)–(e) Corresponding transversally-averaged spectral intensity along z for (c) one, (d) two and (e) three unchirped pulses. Insets show characteristic THz fields ($\nu < 80$ THz) in GV m^{-1} versus time in fs at the indicated distances.

To end with, figure 6 displays interesting features related to positive/negative chirp parameters and larger time delays. In figure 6(a), with a positive chirp the THz yield is higher by ~30% than with a negative one. This is justified by the relative phase remaining closer to the optimal value $\pi/2$ at the distance of maximum increase in the THz energy (see vertical dotted line). This property has been counterchecked for different pulse configurations (not shown) and it agrees with the gain factors reported by passing from negative to positive chirps in previous experimental observations [15]. Besides, figure 6(b) illustrates the efficiency of two unchirped pulses with 4.5 mJ energy separated by a large delay $\Delta t = 2\tau$. This sequence of two pulses achieves a 3.5 higher THz yield over distances <1 m, leading to important laser-to-THz conversion efficiencies $>10^{-4}$ (see inset of

figure 6(b)). The THz field first develops modulations over 2τ period induced by the early ionization of air. Later, the second pulse lengthens plasma generation initiated by the first pulse. Comparing figures 6(c), (d) and their insets thus suggests that it is possible to control the shape and intensity of the THz spectra from using double-pulsed laser fields. Similar patterns can be exploited with three delayed pulses, which supply higher spectral intensities over broad spectral ranges (figure 6(e)).

These simulations show that working with wavetrains of femtosecond light pulses can provide experimentalists with flexible tools for engineering THz pulses and spectra for various spectroscopic purposes. One possible setup is first to extract SH from, e.g., a BBO crystal, configure its duration and polarization state through appropriate gratings and half-wave plates, and couple it collinearly to FH using a delay line [34]. The next step would then consist in launching the resulting two-color pulse into the experimental layout exploited in [11], i.e., forming replicas of the two-color pulses by means of a Mach–Zehnder type interferometer introducing a second pulse at variable delay Δt.

5. Conclusion

To summarize, THz emissions by two-color pulses can be engineered through chirping and multi-pulse techniques. 3D simulations of two, delayed and chirped dual-color pulses displayed evidence of a net increase in the laser-to-THz conversion efficiency in focused propagation geometry, compared with a single, chirped Gaussian pulse. We provided a simple criterion allowing to estimate the potential improvement of complex input waveforms onto the laser-to-THz conversion efficiency based on the knowledge of the spectra of the initial laser field and the produced free electron density only. Next, we highlighted the important role of long propagation ranges to fully exploit the potential of chirped pulses. Pulse chirping can be highly beneficial in filamentation setups because it enables a more efficient coupling between the two colors over longer propagation distances. Combining several pulses with appropriate time delays makes the THz energy yield and spectra tunable in both focused and collimated propagation geometries. These techniques should be easily implemented in experimental setups dedicated to THz spectroscopy for remote detection.

Acknowledgments

This work was supported by the ANR/ASTRID Project 'ALTESSE' # ANR-15-ASTR-0009 and performed using HPC resources from GENCI (Grant #2016-057594 and #A0020507594). SS acknowledges support by the Qatar National Research Fund through the National Priorities Research Program (Grant # NPRP 8-246-1-060).

ORCID iDs

S Skupin https://orcid.org/0000-0002-9215-1150
L Bergé https://orcid.org/0000-0002-5531-7692

References

[1] Tonouchi M 2007 Cutting-edge terahertz technology *Nat. Photon.* **1** 97
[2] Thomson M D, Kress M, Löffler T and Roskos H G 2007 Broadband THz emission from gas plasmas induced by femtosecond optical pulses: from fundamentals to applications *Laser Photonics Rev.* **1** 349
[3] Giles-Davies A, Burnett A D, Fan W, Linfield E H and Cunningham J E 2008 Terahertz spectroscopy of explosives and drugs *Mater. Today* **11** 18
[4] Vicario C, Monoszlai B and Hauri Ch P 2014 GV/m single-cycle terahertz fields from a laser-driven large-size partitioned organic crystal *Phys. Rev. Lett.* **112** 213901
[5] Kim K Y, Taylor A J, Glownia J H and Rodriguez G 2008 Coherent control of terahertz supercontinuum generation in ultrafast laser–gas interactions *Nat. Photon.* **2** 605
[6] Clerici M *et al* 2013 Wavelength scaling of terahertz generation by gas ionization *Phys. Rev. Lett.* **110** 253901
[7] Nguyen A, González de Alaiza Martínez P, Déchard J, Thiele I, Babushkin I, Skupin S and Bergé L 2017 Spectral dynamics of THz pulses generated by two-color laser filaments in air: the role of Kerr nonlinearities and pump wavelength *Opt. Express* **25** 4720
[8] Babushkin I, Skupin S, Husakou A, Köhler C, Cabrera-Granado E, Bergé L and Herrmann J 2011 Tailoring terahertz radiation by controlling tunnel photoionization events in gases *New J. Phys.* **13** 123029
[9] Zhang L, Wang G L and Zhou X X 2016 Optimized two- and three-colour laser pulses for the intense terahertz wave generation *J. Mod. Opt.* **63** 2159
[10] Ravi K, Schimpf D N and Kärtner F X 2016 Pulse sequences for efficient multi-cycle terahertz generation in periodically poled lithium niobate *Opt. Express* **24** 25582
[11] Vicario C, Ovchinnikov A V, Chefonov O V and Hauri C P 2016 Multi-octave spectrally tunable strong-field terahertz laser arXiv:1608.05319
[12] Liu J, Dai J, Chin S L and Zhang X-C 2010 Broadband terahertz wave remote sensing using coherent manipulation of fluorescence from asymmetrically ionized gases *Nat. Photon.* **4** 627

[13] Daigle J-F, Théberge F, Henriksson M, Wang T-J, Yuan S, Châteauneuf M, Dubois J, Piché M and Chin S L 2012 Remote THz generation from two-color filamentation: long distance dependence *Opt. Express* **20** 6825
[14] Wang T-J, Yuan S, Chen Y, Daigle J-F, Marceau C, Théberge F, Châteauneuf M, Dubois J and Chin S L 2010 Toward remote high energy terahertz generation *Appl. Phys. Lett.* **97** 111108
[15] Wang T-J, Chen Y, Marceau C, Théberge F, Châteauneuf M, Dubois J and Chin S L 2009 High energy terahertz emission from two-color laser-induced filamentation in air with pump pulse duration control *Appl. Phys. Lett.* **95** 131108
[16] Wang W M, Sheng Z M, Wu H C, Chen M, Li C, Zhang J and Mima K 2008 Strong terahertz pulse generation by chirped laser pulses in tenuous gases *Opt. Express* **16** 16999
[17] Babushkin I, Kuehn W, Koehler C, Skupin S, Bergé L, Reimann K, Woerner M, Herrmann J and Elsaesser T 2010 Ultrafast spatiotemporal dynamics of terahertz generation by ionizing two-color femtosecond pulses in gases *Phys. Rev. Lett.* **105** 053903
[18] Jefimenko O D 1966 *Electricity and Magnetism: An Introduction to the Theory of Electric and Magnetic Fields* (New York: Appleton-Century-Crofts)
[19] Amico C D, Houard A, Akturk S, Liu Y, Le Bloas J, Franco M, Prade B, Couairon A, Tikhonchuk V and Mysyrowicz A 2008 Forward THz radiation emission by femtosecond filamentation in gases: theory and experiment *New J. Phys.* **10** 013015
[20] Andreeva V A *et al* 2016 Ultrabroad terahertz spectrum generation from an air-based filament plasma *Phys. Rev. Lett.* **116** 063902
[21] Kolesik M, Moloney J V and Mlejnek M 2002 Unidirectional optical pulse propagation equation *Phys. Rev. Lett.* **89** 283902
[22] Kolesik M and Moloney J V 2004 Nonlinear optical pulse propagation simulation: From Maxwell's to unidirectional equations *Phys. Rev.* E **70** 036604
[23] Bergé L, Skupin S, Nuter R, Kasparian J and Wolf J P 2007 Optical ultrashort filaments in weakly-ionized, optically-transparent media *Rep. Prog. Phys.* **70** 1633
[24] Peck E R and Reeder K 1972 Dispersion of air *J. Opt. Soc. Am.* A **62** 958
[25] Wahlstrand J K, Cheng Y H and Milchberg H M 2012 Absolute measurement of the transient optical nonlinearity in N_2, O_2, N_2O, and Ar *Phys. Rev.* A **85** 043820
[26] Zahedpour S, Wahlstrand J K and Milchberg H M 2015 Measurement of the nonlinear refractive index of air constituents at mid-infrared wavelengths *Opt. Lett.* **40** 5794
[27] Perelomov A M, Popov V S and Terent'ev M V 1966 Ionization of atoms in an alternating electric field *Sov. Phys. JETP* **23** 924 (www.jetp.ac.ru/cgi-bin/dn/e_023_05_0924.pdf)
[28] Bergé L, Soulez C L, Koehler C and Skupin S 2011 Role of the carrier-envelope phase in laser filamentation *Appl. Phys.* B **103** 563
[29] González de Alaiza Martínez P, Babushkin I, Bergé L, Skupin S, Cabrera-Granado E, Köhler C, Morgner U, Husakou A and Herrmann J 2015 Boosting terahertz generation in laser-field ionized gases using a sawtooth wave shape *Phys. Rev. Lett.* **114** 183901
[30] Li M, Li W, Shi Y, Lu P, Pan H and Zeng H 2012 Verification of the physical mechanism of THz generation by dual-color ultrashort laser pulses *Appl. Phys. Lett.* **101** 161104
[31] Thiele I, González de Alaiza Martínez P, Nuter R, Nguyen A, Bergé L and Skupin S 2017 Broadband terahertz emission from two-color femtosecond-laser-induced microplasmas *Phys. Rev.* A **96** 053814
[32] Andreeva V A, Esaulkov M, Panov N, Solyakin P, Makarov V, Shipilo D, Shkurinov A, Kosareva O and Chin S L 2016 *Conf. on Lasers and Electro-Optics* (Washington, DC: OSA) p JW2A.47
[33] Nuter R and Bergé L 2006 Pulse chirping and ionization of O_2 molecules for the filamentation of femtosecond laser pulses in air *J. Opt. Soc. Am.* B **23** 874
[34] Xie X, Dai J and Zhang X C 2006 Coherent control of THz wave generation in ambient air *Phys. Rev. Lett.* **96** 075005